ASTM INTERNATIONAL

Geotechnical Testing Journal

Yi Dong[1] and Ning Lu[2]

DOI: 10.1520/GTJ20190357

Measurement of Suction Stress and Soil Deformation at High Suction Range

Geotechnical Testing Journal

doi:10.1520/GTJ20190357 available online at www.astm.org

Yi Dong[1] and Ning Lu[2]

Measurement of Suction Stress and Soil Deformation at High Suction Range

Reference

Y. Dong and N. Lu, "Measurement of Suction Stress and Soil Deformation at High Suction Range," *Geotechnical Testing Journal* https://doi.org/10.1520/GTJ20190357

ABSTRACT

Suction stress is the effective stress independent of mechanical boundary conditions but is due to water content variation. It occurs on or near particle contacts and does not directly transfer through the soil skeleton and hence can only be and has been measured indirectly and deduced from soil's strength or deformation. In this work, a new technology to measure the soil-water retention curve, soil shrinkage curve, and suction stress characteristic curve in a high suction environment is established. A humidity-controlled device to measure suction stress was developed based on a previously established drying cake method. Nitrogen gas and molecular sieves were introduced as desiccant in addition to saturated salt solutions to generate an extreme dry environment up to 850 MPa of matric suction for the first time. A focus on the effect of adsorptive soil-water interaction on hydromechanical properties of expansive soils provides enriched information on elastic modulus variation, soil deformation evolution, and matric suction development of soil in very low water contents, making the suction stress measurement possible for matric suction as high as 850 MPa.

Keywords

unsaturated soil, suction stress, soil shrinkage, soil-water retention curve, relative humidity, vapor equilibrium, high suction, molecular sieve

Manuscript received October 1, 2019; accepted for publication January 10, 2020; published online March 4, 2020.

[1] State Key Laboratory of Geomechanics and Geotechnical Engineering, Institute of Rock and Soil Mechanics, Chinese Academy of Sciences, Xiaohongshan 2, Shuiguohu St., Wuhan, Hubei 430071, China (Corresponding author), e-mail: ydong@whrsm.ac.cn, https://orcid.org/0000-0003-1237-0079

[2] Department of Civil and Environmental Engineering, Colorado School of Mines, 1600 Illinois St., Golden, CO 80401, USA, https://orcid.org/0000-0003-1753-129X

Introduction

Interparticle stresses among soil grains caused by water content variation play a significant role in soil deformation (Lu and Dong 2017) and stiffness (Dong and Lu 2016) during the drying or wetting process. The origin of this type of interparticle stress, associated with the energy state of the system of soil matrix and pore water, has been identified from two soil-water interaction mechanisms (i.e., Lu and Likos 2006; Lu and Khorshidi 2015): capillary interaction that occurred because of the existence of curved air-water interfaces and

adsorptive interaction that occurred because of the adsorption of water on or within particle surfaces or soil mineral. The local interparticle stresses, including capillary attraction caused by surface tension, lowered pore water pressure, van der Waals attraction induced from surface adsorption, electrostatic attraction by ion hydration, electrical double-layer repulsion, and other physicochemical interactions, can be lumped into a conceptualized "suction stress" (Lu and Likos 2006). The dependency of suction stress on water content represents the intrinsic feature of the interparticle stress development, and this relationship can be defined as the suction stress characteristic curve (SSCC) (Lu and Likos 2006). SSCC has been demonstrated to be intercorrelated with the soil-water retention curve (SWRC), and SSCC and SWRC are the two most important constitutive relationships describing the hydrological and mechanical behaviors for unsaturated soils (Lu and Likos 2004; Lu, Kaya, and Godt 2014).

However, the determination of interparticle stresses or suction stress because of adsorption is relatively new compared with suction stress because of capillarity. For soils at a high water content or low matric suction state in which capillarity dominates the soil-water interactions, the effective degree of saturation has been satisfactorily used to define suction stress upscaling from the air-water interfaces to the representative element volume of soil (e.g., Lu and Likos 2004; Lu, Godt, and Wu 2010; Alonso et al. 2010; Greco and Gargano 2015). Among those, the effect of adsorption on the effective stress has been cast in some similar concepts as certain residual water content (e.g., microscopic degree of saturation, irreducible pore water fraction, and wetted external surface ratio, etc.). Notwithstanding, the vagueness of the concept of residual water content and the incompleteness of the definition of pore water pressure for soils at low water content or high suction range have been recently recognized (Lu and Zhang 2019; Zhang and Lu 2019). The use of residual water content increases the uncertainty of the distinction of suction stress in capillary or adsorptive regimes. On the other hand, at low water content or high matric suction state, suction stress is mostly induced by adsorptive water interaction, particularly in silty and clayey soils, and has been historically neglected (e.g., Bishop's effective stress (Bishop 1959) only uses capillary pressure and does not consider adsorption) or simplified as a constant value within the residual water content (e.g., suction stress using residual water content in Lu, Godt, and Wu 2010). Therefore, the determination of suction stress at high suction range or adsorptive water retention regime is necessary and useful, both experimentally and theoretically, for mechanical behaviors of soil, particularly clayey and silty soil, under very dry conditions in various geotechnical applications (e.g., geothermal energy recovery or nuclear waste repository, or soil cracking in arid landscapes).

Suction stress, as an interparticle stress, is an active effective stress independent of the external loading or constraining boundary conditions but is dependent on water content and nontransferable through the soil skeleton (Lu and Dong 2017). Its mechanical manifestation for soils with decreasing suction stress is the enhancement of strength and the augment of stiffness. Hence, it can be handily inferred indirectly from the strength measurement or deduced from deformation measurements. The former approach usually tests the shear strength by triaxial or direct shear (e.g., Khosravi et al. 2012; Alsherif and McCartney 2014) or tensile strength by uniaxial tension test or Brazilian tension test (e.g., Lu, Wu, and Tan 2007; Akin and Likos 2017). These methods are destructive methods that can only offer one strength value for a soil sample under the single value of water content or matric suction and therefore introduce uncertainties for soil sample preparation at various water contents and matric suction values. They are subject to inconsistency on suction stress measurements. Alternatively, nondestructive methods continuously record some measurable quantities, such as deformation and modulus, and then infer the interparticle stress by applying assumptions of elasticity. Nondestructive methods include the restrained ring method (Abou Najm et al. 2009), triaxial K_0 method (Oh et al. 2013), and drying cake method (Lu and Kaya 2013; Dong and Lu 2017).

Nevertheless, all methods are involved in complex instrumentations or require a long time for equilibrium, and they are all constrained by a limited range of controllable matric suction. The highest suctions so far can be made using a vaporization equilibrium technique by salt solution or vapor condensation technique is about 374 MPa (6.6 % of relative humidity (RH) by saturated lithium bromide (LiBr) solution) or 412 MPa (~5 % of RH (Likos and Lu 2003) and by Vapor Sorption Analyzer, Decagon Devices Inc., Pullman, WA

(Likos, Lu, and Wenszel 2011)). For clayey soils, the water can still reside in nanopores of soil particles in the form of adsorptive water, e.g., about 5 % of water by mass in bentonite or smectite under RH of 5 % condition (Likos and Lu 2003). Hence, the behaviors of SWR and SSCC for soil from suction higher than 412 MPa or RH lower than 5 % in oven-dried conditions are intriguing and are imperative for understanding the effects of clay water adsorption on its mechanical and hydraulic behaviors, which also have implications for heat and mass transfer in subsurface energy management and water dynamics and migration in buffering materials of clays for solid waste repository.

In this work, we follow the nonfailure and deformation-based methodology invented by Lu and Kaya (2013) to design a well-controlled environmental chamber using 4Å molecular sieves (MS) to attain suction as high as 850 MPa (0.21 % of RH). Four types of expansive soils are tested under zero total stress conditions, and their suction stresses and deformations are measured and analyzed. The capability of measuring SSCC and soil shrinkage curve (SSC) using this technology is demonstrated and will be described in the following sections.

Experimental Design and Testing Procedure

ENVIRONMENTAL CHAMBER

The experimental design on the RH controlled environmental chamber is presented in figure 1. The system consists of a sealed container, digital balances, and digital cameras. The container is made by transparent acrylic plate with 5.08 cm of thickness to reduce the temperature fluctuation inside. A digital balance with 0.001 g accuracy (WKC603C, Mettler Toledo, Inc.) is placed inside of the chamber and connected to the computer. The system is capable of testing two soil samples simultaneously with two balances and two cameras. For simplicity, only one set of soil sample measurement is presented in figure 1. The soil sample is placed at the center of the balance platform. The top plate of the container is transparent, and a digital camera is positioned above the balance for image shooting. A light-emitting diode light strip is stuck on the top plate to provide consistent illumination and remove shadows to get the best quality of the image. A humidity/temperature sensor (DMT340, Vaisala Corporation) is mounted on the wall of the container and connected to a personal computer to monitor the RH change and temperature fluctuation. A small fan is installed inside the chamber to accelerate air circulation. A reservoir is seated at the corner inside the chamber for salt solution. A plastic tube with a ball valve is inserted into the chamber to vent the air when purging nitrogen gas and to deliver/remove salt solution to/from the reservoir at the intermediate steps of drying. An air hose with a stopper is connected to a gas-drying cylinder filled with MS and to a nitrogen gas tank to provide dry air into the chamber for the final step of the driest condition in the desiccating process.

FIG. 1

Schematic illustration of the experimental setup for high suction control. LED = light-emitting diode; PC = personal computer.

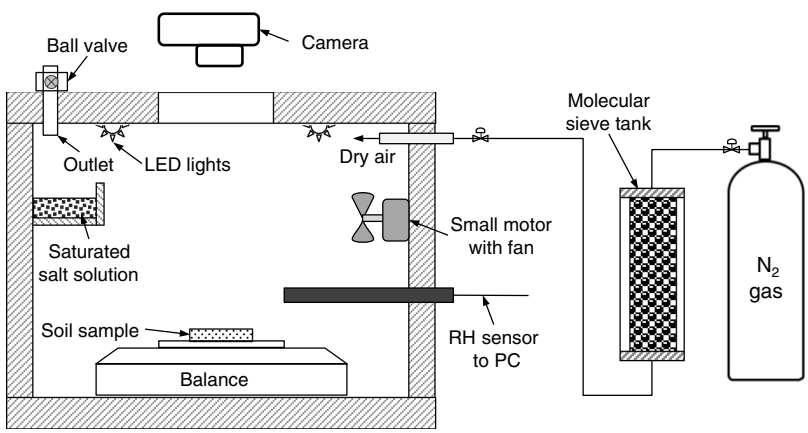

MS REACTIVATION

MS are materials with nanopores of uniform size that are commonly seen in purifying gas streams in the petroleum industry and solvent drying in analytical chemistry or catalytic applications. MS appear to have an ultra-strong capability of water vapor adsorption yet a moderate adsorption capacity (~25 % by mass). A 4Å zeolite MS purchased from ZEOCHEM is used as an aggressive desiccant. The received product is usually fully saturated under room temperature/humidity conditions and therefore needs to be reactivated or regenerated before use. A certain amount of MS (e.g., 500 g) was weighed and put in a sealed glass flask with flow control adaptor. The flask was then heated using a bunsen burner to above ~300°C under a vacuum for 10–30 min to remove the adsorbed water molecules in MS nanopores. The total weight was recorded for the dry mass of the MS. The flask was cooled and refilled with dry nitrogen gas, and then the MS was quickly transferred to a sealed gas-drying cylinder for later use.

SOIL PREPARATION

To test the methodology, a total of four clayey soil samples representing low-expansive (Sanmenxia clay), expansive (Denver claystone and Boulder clay), and high-expansive (Ningming clay), classified by McKeen (1992), were selected for the measurements. Table 1 lists the initial porosities and the unified soil classifications for the samples examined. All soils were pulverized and oven dried before use. A certain amount of soil powder was compacted into a thin cake sample with a diameter of 32.5 mm and thickness of 7.5 mm. Two identical soil cake samples were prepared for each type of soil, wherein one cake was dried in the environmental chamber to determine deformation and suction stress, and the other cake was dried in a similar apparatus imbedded in a mini-loading system to measure the elastic modulus (see details in Dong and Lu 2017).

Next, soil cakes were deaired in a desiccator under vacuum for at least 2 h. Then, deaired water was gradually imported into the desiccator until the samples were inundated, and samples were saturated under a vacuum for 24 h. After saturation, the samples were carefully extruded out of the cylinder mold and transferred onto a circular sample holder. A thin grease film was spread between the soil cake and holder to reduce friction. This treatment is important for the removal of any constraint on the boundary of the soil cake so that the sample deforms freely without developing cracks under various environmental loadings. The digital camera was then center-aligned with the soil cake and ready for testing.

DRYING PROCESS

The general procedures followed the same working principle as previously established in Lu and Kaya (2013) and Dong and Lu (2017). The test began as the soil cake was placed on the balance and the environmental chamber was closed to let the sample slowly dry. The digital balance monitored the change of weight throughout the entire test, and thus the variation of water content can be calculated. The RH and temperature sensor recorded real-time RH and temperature variation. The digital camera took images with an interval of ~5 % degree of saturation decrement at every drying step. The image postprocesses allowed the determination of the volume change of soil cake during drying. A small fan was only needed right after the RH change to speed up the circulation of the moist

TABLE 1

Geotechnical properties, hydromechanical parameters, and deformation parameters for tested soils

					Geotechnical Index, %			SWRC Parameters					Shrinkage
#	Soils	Abbreviation	USCS	Porosity	LL	PL	PI	w^a_{max}	α	n	SSA, m^2/g	CEC, meq/g	Characteristics, $\partial e/\partial m$
1	Boulder clay	BoC	CL	0.435	44.4	21.7	22.7	0.056	6.453	2.543	…	…	0.111
2	Denver claystone	DCs	CL	0.536	44.9	25.4	19.5	0.053	27.29	1.557	152.64	0.35	0.165
3	Sanmenxia clay	SmC	ML	0.484	35.6	19.3	16.3	0.062	4.159	2.683	…	…	0.055
4	Ningming clay	NmC	CH	0.567	159.4	37.5	121.9	0.130	3.369	1.455	…	…	0.217

Note: CEC = cation-exchange capacity; LL = liquid limit; PI = plasticity index; PL = plastic limit; SSA = specific surface area; USCS = Unified Soil Classification System; ML = silt; CL = clay of low plasticity; CH = clay of high plasticity.

air and accelerate the equilibrium of moisture. **Figure 2** presents drying out curves of the soil obtained during a multistep drying process. For the first drying step, the RH was set in the range from 98 to 99 %, which is equivalent to around 1 to 2 MPa of total suction, so that soil-water evaporated slowly out of the sample. This RH can be generated by employing pure liquid water or saturated potassium sulfate solution in the reservoir inside the chamber. Hydrophobic silane regent was painted on the inner wall of the top plate to avoid condensation of water vapor so the top plate would be transparent for the photos. The first drying step may evaporate the majority of capillary water, depending on soil type, and the water content can be reduced to lower than half of its initial saturated water content. The camera took a number of images to record the soil cake deformations. The first drying step was not completed until the soil weight barely changed and reached an equilibrium state. The following drying steps proceed by controlling the RH close to the room RH condition (~50 %) by using saturated potassium carbonate solution (44.3 % of RH), and the next drying step is ~10 % of RH by using saturated LiBr solution (6.37 % of RH). The discrepancies of the RH at equilibrium from the theoretical RH values of the saturated solutions stem from the limited amount of saturated salt solutions placed in the chamber.

Beyond the drying capability of the salt solution, the last drying step of the test was achieved using MS. In this step, saturated salt solution was removed from the chamber, and MS stored in a gas-drying cylinder was connected to the chamber and the nitrogen gas tank. The nitrogen gas further dried through the MS cylinder was purged into the environmental chamber. The adsorption isotherm provided by the MS manufacturer is presented in **figure 3**. The curve presents the relationship between absorbed water content and equilibrated

FIG. 2

Variation of volumetric water content with time and the corresponding RH during the stepwise drying process for (*A*) Boulder clay (BoC) and Denver claystone (DCs) and (*B*) Sanmenxia clay (SmC) and Ningming clay (NmC).

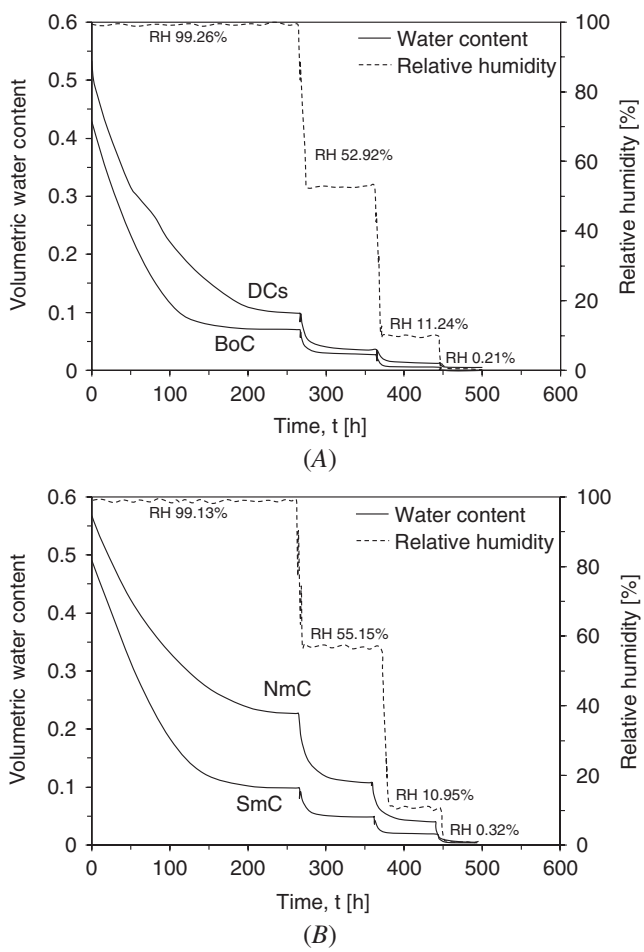

FIG. 3

Determination of the highest suction using MS based on sorption isotherm from the MS manufacture.

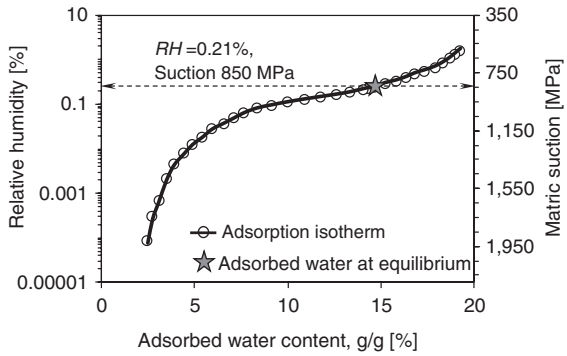

RH of the MS under room temperature conditions (20°C). The star indicates the driest state acquired in this test, which compares well with the reading from the RH sensor. The lowest RH or highest suction obtained by using MS is 0.21 % or 850 MPa. The entire drying scheme was designed by combining the vapor equilibrium technique of salt solution (from saturation to ~10 % of RH) and trace water adsorption technique by MS (below ~10 % of RH). This is for the consideration that the RH between 10 and 99 % took quite a large proportion of the drying time consumption and evaporated a large portion of pore water, which can be easily achieved by conventional saturated salt solution so that ineffective use of nitrogen gas and inefficient consumption of MS were avoided. Because of the inadequate adsorption capacity of MS and higher requirement of the sealing for the connections and compartments, it was only applied at the last drying step to maintain a very dry air condition.

Results

Examples of progressive drying curves of four tested soils are shown in **figure 2**. The total drying process usually takes about 2 to 3 weeks, depending on soil type. The intentionally slowed drying process and friction-free boundary condition ensure the homogeneous distribution of water content throughout the sample and enable the soil cake to keep its integrity without cracking. All measurements are summarized and discussed as follows.

SOIL DEFORMATION

The changes of cross section area of the cake sample are obtained through image processing. The radial strain, as a function of water content, can be determined as the ratio between cumulative changes of diameter from current water content to the initial diameter at saturated condition. The thickness of the soil cake at different water contents can be identified through the separate elastic modulus measurement on the other cake sample. The drying cake test for each soil has been conducted twice to validate that the variability of deformation between these two samples is trivial. The actuator of the mini-loading system recorded the position at which the loading plate fully contacted the soil cake sample. Hence, the thickness of the sample can be converted (see details in Dong and Lu 2017). Given the measured diameters and thicknesses at various water contents, the variation of volumetric strain can be calculated.

The comparisons of the developments of total or accumulative radial strain, vertical strain, and volumetric strain as the water content changes are presented in **figure 4**. Positive strain values represent shrinkage deformation. It is shown that the radial strain and vertical strain are almost identical and are approximately one third of the total volumetric strain at any water content, which indicates that the deformations during drying are isotropic and homogeneous. The maximum total drying shrinkage varies from 0.12 for low-expansive clay (Sanmenxia clay) to 0.25 and 0.28 for expansive clay (Boulder clay and Denver claystone, respectively) and can reach up to

FIG. 4 Cumulative strains of four soil samples during drying: (*A*) Boulder clay (BoC), (*B*) Denver claystone (DCs), (*C*) Sanmenxia clay (SmC), and (*D*) Ningming clay (NmC).

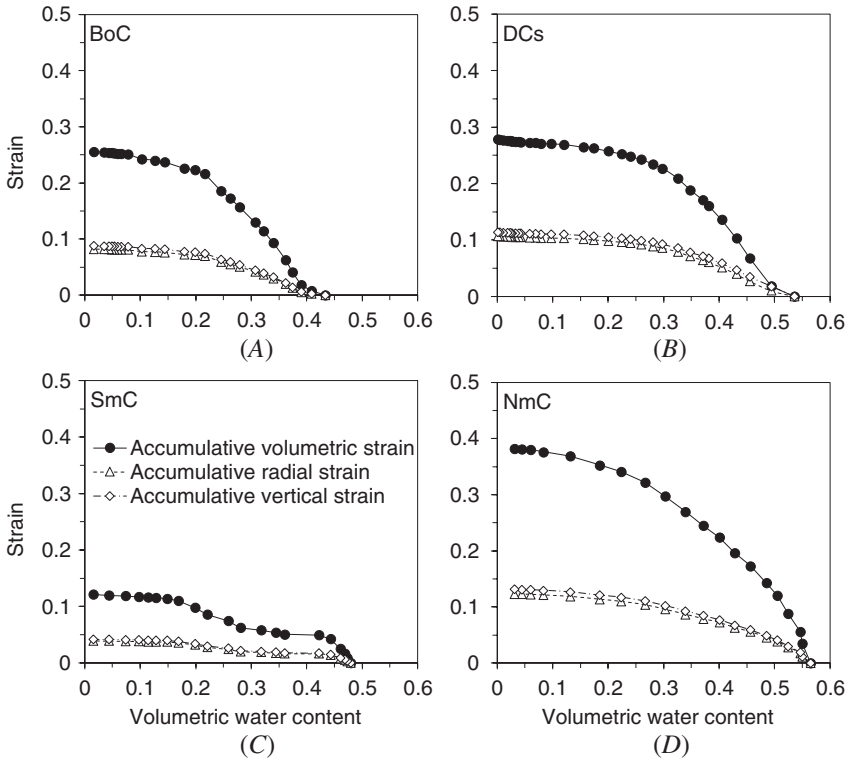

0.38 for high-expansive clay (Ningming clay). Soils shrink continuously and strains increase monotonically as the water content decreases during drying. Continuous shrinkage strain can also be observed as the soils dry in the low water content range. Note that although clayey soils may undergo remarkable deformation under surcharge, zero total stress conditions are applied so that the soil shrinkage is considered induced only by suction stress, which depends on soil-water content.

Another interpretation of soil deformation because of drying is the characteristic SSC, defined as the relationship between void ratio and moisture ratio (the ratio of volume of water to volume of solid, m). The soil shrinkage curve quantifies the deformation of a soil under zero total stress conditions induced only by suction stress. Because of the dependency of suction stress on soil-water content, there exists an intrinsic intercorrelation between SSC and SWRC (Lu and Dong 2017). **Figure 5** presents the SSCs for four tested soils in this study. The moisture ratio helps to compare both the volume of voids and water relative to the volume of soil particles. The diagonal dash lines indicate the fully saturated condition of soil where the total volume change of void equals or fully attributes to the volume change of pore water. It shows that the void ratios decrease firstly along the saturation line and then deviate after the air entry and the slopes of SSC gradually decrease. Two different water retention regimes, namely capillary and adsorptive regimes, can be differentiated based on the variation of the slope of SSC as the moisture ratio decreases (Lu and Dong 2017). As the soil approaches the dry end, the constant slope or nonzero shrinkage rate, defined by change of void ratio per moisture ratio, can be observed from the SSC. The shrinkage rates, $\partial e/\partial m$, in the range of low moisture ratio for all tested soils are listed in **Table 1**. In accordance to the correlation identified by Lu and Dong (2017) for the shrinkage rate and soil index properties, more clayey soils with higher liquid limit values present larger shrinkage rates at low water content. This suggests that expansive soil containing more fine content shows stronger adsorption effects, more hydrated water exists

FIG. 5

SSCs of four soils tested: (*A*) Boulder clay (BoC), (*B*) Denver claystone (DCs), (*C*) Sanmenxia clay (SmC), and (*D*) Ningming clay (NmC).

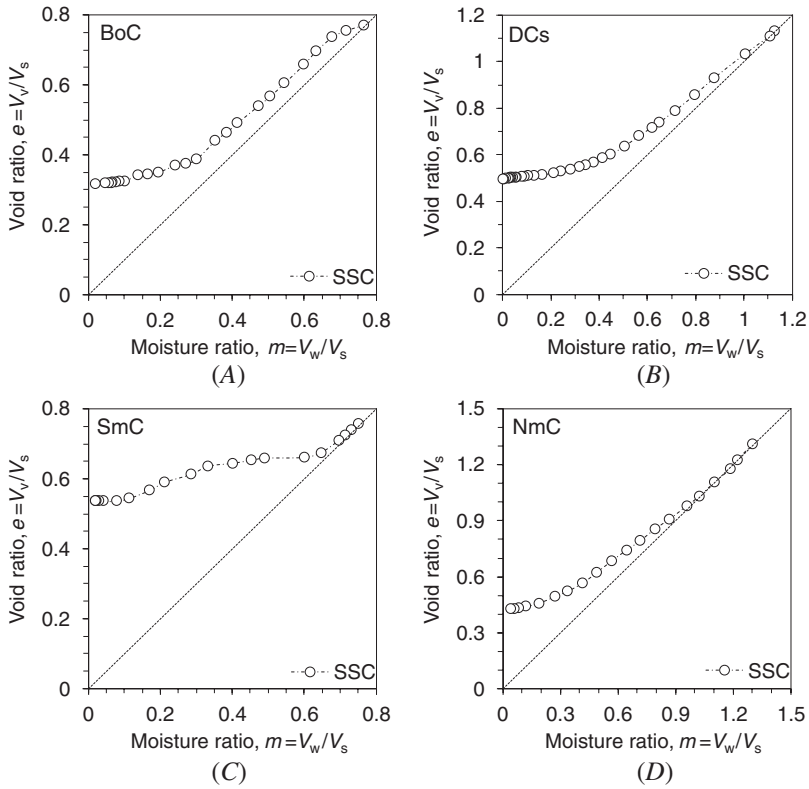

between the silicate interlayers and on the particle surface, and, correspondingly, the soil becomes more expansive with a more pronounced shrinkage rate.

ELASTIC MODULUS

The elastic Young's moduli of soil cakes $E(\theta)$ are measured independently using a separate mini-loading apparatus (Lu and Dong 2017). An actuator with minimum moving speed of 0.12 μm/s and maximum thrust of 540 N (Zaber Technologies Inc.) compresses the soil cake slowly without horizontal constraint, and an accurate S-beam load cell records the compressive force. The slope of the linear portion of the uniaxial stress and vertical strain curve was determined as elastic Young's modulus. The moduli are measured at varying water contents individually with the drying cake measurement. For the convenience of data analysis, the soil cake for elastic modulus are dried synchronized with the soil cake for deformation measurement. In other words, the water contents for elastic modulus measurement are selected as the same as water contents for SSC. **Figure 6** presents the measured elastic modulus evolution for four different soils under drying. It shows that the elastic modulus tends to increase nonlinearly and monotonically as the water content decreases. The modulus in low water content can be found to continuously increase as the water content decreases, rather than keeping constant. For instance, Boulder clay increases 10 % of its maximum elastic modulus from 1.95 to 2.16 MPa in the residual 10 % of the saturation as the water content decreases from 0.049 to 0.016; Denver claystone also increases 3.4 % of the modulus in residual 7 % of the water, i.e., from 2.56 to 2.65 MPa as the water content decreases from 0.039 to 0.001. Sanmenxia clay and Ningming clay show relatively small development on elastic modulus as water content decreases in the range of low water content, comparing with Boulder clay and Denver claystone. Sanmenxia clay develops ~50 % of the stiffness from saturation to 88 % of saturation, and then increases the modulus from 1.17 to 2.06 MPa as the water content decreases from 0.42 to 0.01. Similarly, Ningming clay attains 80 % of the total stiffness to 1.79 MPa as the

FIG. 6

Young's modulus functions of soils tested: (*A*) Boulder clay (BoC), (*B*) Denver claystone (DCs), (*C*) Sanmenxia clay (SmC), and (*D*) Ningming clay (NmC).

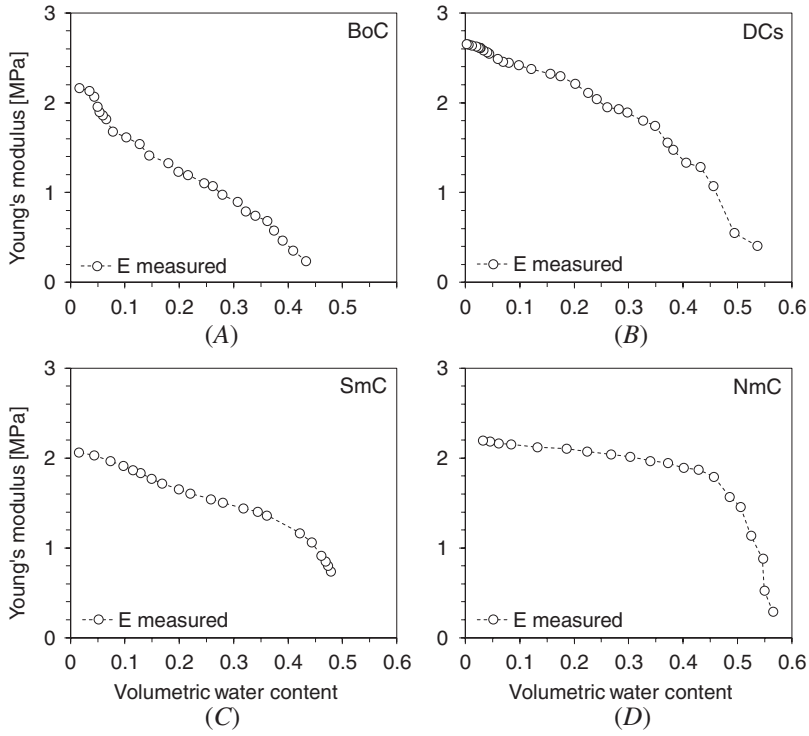

water content decreases from saturation to 80 % degree of saturation and then develops the remaining 20 % of the modulus to 2.19 MPa as the water content decreases from 0.45 to 0.03. The maximum elastic modulus at driest conditions is in the range between 2 and 3 MPa and varies depending on soil type.

SUCTION STRESS DETERMINATION

Rational assumption of uniformly distributed water content throughout the soil sample during drying leads to suction stress evolving isotropically and identically at every point inside the cake sample. Therefore, the soil cake can be representative as a single soil element. Given by the information of soil deformation and modulus during drying, the interparticle stress or suction stress can be directly deduced from known $E(\theta)$ and SSC as follows (Lu and Dong 2019):

$$\sigma^{s} = \frac{E \cdot \varepsilon_{t}}{3(2\nu - 1)} \tag{1}$$

where σ^{s} is the suction stress in soil, E is the elastic modulus function, and ε_{t} is the total volumetric strain, and ν is the Poisson's ratio assumed to be a constant of 0.25 for all soils at any water content. Lu and Dong (2019) derived the SSCC in incremental form as stress contributed by the shrinkage deformation and stress contributed by the increase of stiffness:

$$\Delta\sigma^{s} = \frac{E}{3(2\nu - 1)}\Delta\varepsilon_{t} + \frac{\varepsilon_{t}}{3(2\nu - 1)}\Delta E \tag{2}$$

where $\Delta\sigma^{s}$ is the incremental suction stress between two water contents, ΔE is the incremental modulus change, and $\Delta\varepsilon_{t}$ is the incremental change of total volumetric strain. Converting volumetric strain into void ratio by

$\Delta e = \varepsilon_t/(1-n)$, where n is the initial porosity under fully saturated conditions, the complete form of total suction stress at given water content can be formulated as follows:

$$\sigma^s = \sum_m \Delta\sigma^s = \frac{E}{3(2\nu-1)}\sum_m \Delta(\Delta e(1-n)) + \frac{\Delta e(1-n)}{3(2\nu-1)}\sum_m \Delta E \tag{3}$$

The measured suction stress characteristic curves using equations (1)–(3) are presented in **figure 7**. A negative sign of suction stress indicates tensions that tend to pull soil particles together. It shows that the developments of suction stress because of soil drying are highly nonlinear and are similar in patterns with the development of soil deformation (**fig. 4**) and elastic modulus function (**fig. 6**). For expansive clays, suction stress decreases continuously as soil dries. However, for nonexpansive kaolinite or sand, suction stress first decreases, then increases in the range of low water content (Lu and Dong 2017). The magnitude of suction stress developed because of drying also varies depending on soil type. The lowest suction stress in Sanmenxia clay can be −172 kPa, while Denver claystone and Boulder clay can develop −312 and −383 kPa of suction stress, respectively. The lowest suction stress in the most expansive Ningming clay is −594 kPa. Generally, the lower suction stress can be developed in more expansive soils because of drying caused by more intensive capillary effects on higher content of fine particles and stronger physicochemical interactions in clay water adsorption. **Figure 7** also reveals that in the low water content range, suction stress is not a constant value but slightly evolves at varying water content. Specifically, suction stress changes from −345 to −383 kPa as the water content decreases from 0.05 to 0.01 in Boulder clay; suction stress can further decrease from −309 to −312 kPa as water content reduces from 0.01 to 0.001 for Denver claystone. Sanmenxia clay and Ningming clay show a subtle decrease of suction stress by 4.4 kPa as water content decreases from 0.04 to 0.01 and 10.2 kPa as water content decreases from 0.04 to 0.03. This suggests that in the adsorption water retention regime, adsorptive interaction not only changes the stiffness of the clay material but also contributes to the attractive forces between interlayers and at particle contacts.

FIG. 7

Measured SSCCs based on bulk deformation solution for soils under drying conditions: (*A*) Boulder clay (BoC), (*B*) Denver claystone (DCs), (*C*) Sanmenxia clay (SmC), and (*D*) Ningming clay (NmC).

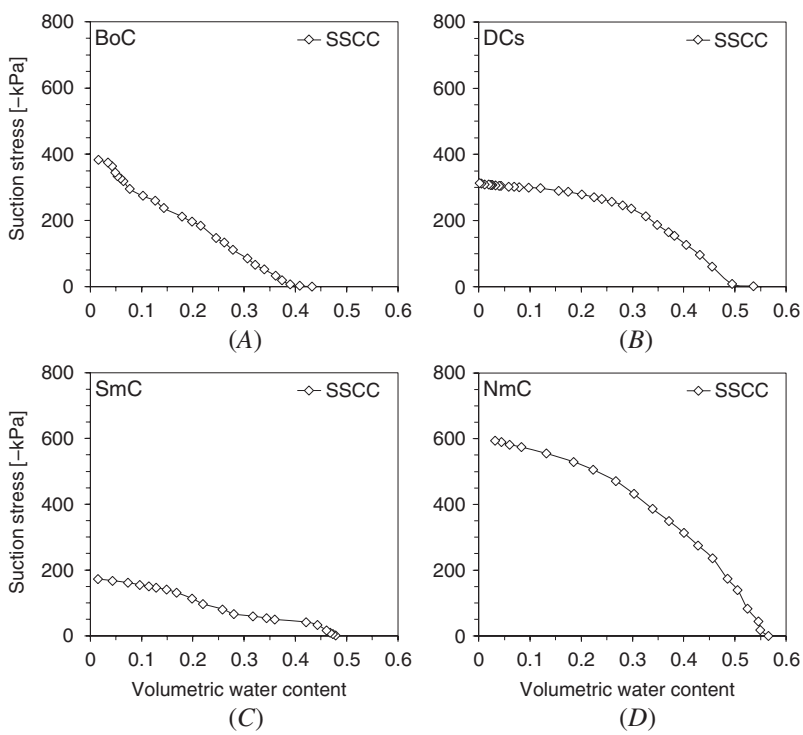

The different changing rates of suction stress at different soil-water retention regimes imply distinct contribution mechanisms for adsorptive water and capillary water to the interparticle stresses. In the capillary water regime, suction stress can be affected more by the pore geometry and boundary conditions, whereas in the adsorptive water regime, soil fabric and mineral characteristics may more strongly influence the development of interparticle forces.

SWRCs

To better analyze soil-water retention behavior, the SWRC model of Lu (2016) was used to fit the experimental data. This model differentiates capillary water and adsorptive water using six fitting parameters with solid physical meanings. The upper bound of both adsorption and capillarity are considered, i.e., the highest matric suction as the limit of adsorption and the cavitation suction as the boundary of capillarity. This model calculates the total gravimetric water content $w(\psi)$ as the superposition of adsorptive water content $w_a(\psi)$ and capillary water content $w_c(\psi)$ in equilibrium with the prevailing matric suction. It is formulated as follows:

$$w(\psi) = w_a(\psi) + w_c(\psi) \tag{4}$$

The adsorptive water content is quantified by a modified adsorption model:

$$w_a(\psi) = w_a^{\max}\left\{1 - \left[\exp\left(1 - \frac{\psi_{\max}}{\psi}\right)\right]^M\right\} \tag{5}$$

where $w_a^{\max}$ is the maximum adsorptive water content, M is the adsorption strength depending on the types of soil and cation, and $\psi_{\max}$ is the maximum matric suction providing the upper bound of matric suction. The capillary water is determined by a modified van Genuchten (1980) model of SWRC considering the cavitation effect and replacing residual water content with adsorptive water content:

$$w_c(\psi) = \frac{1}{2}\left[1 - \operatorname{erf}\left(\frac{\psi - \psi_{cav}}{0.25\psi_{cav}\sqrt{2}}\right)\right](w_s - w_a(\psi))\left[1 + (\alpha\psi)^N\right]^{\frac{1}{N-1}} \tag{6}$$

where α and N are the inverse of air-entry suction and the pore size distribution parameter, respectively, and ψ_{cav} is the mean cavitation suction at which capillary water diminishes. Equations (4)–(6) provide a quantitative assessment of the adsorptive water and capillary water. All measured SWRC data are fitted by using the Lu model to identify the values for all parameters. Key parameters α, N, and $w_a^{\max}$ are listed in **Table 1**.

The matric suctions of the four drying steps were directly converted from the measured RH value using Kelvin's equation (Lu and Likos 2004). The RH sensor measured RH values ranging from 0.21 to 99.26 %. The converted matric suction spread over 3 orders of magnitude from 1 to 850 MPa. For each drying step, the sample weight was monitored, and the next step of drying RH or suction was not applied until the weight change was less than 0.01 g per day to ensure the soil reaches equilibrium. These data of matric suction and corresponding gravimetric water content were compared with independently measured matric suction of each soil at various water contents by using WP4C (Decagon Devices, Inc.). The SWRCs and comparisons of different measurements are presented in **figure 8**. It shows that highly nonlinear S-shape variations of soil-water retention behaviors cross almost six orders of magnitude. The measured SWRCs of each soil compare well with the matric suction measured at equilibrium in the current study and validate the state of equilibrium. The highest suction achieved in the current experiment extended the range of suction measurement from the upper limit of WP4C (~300 MPa) to 850 MPa. The development of matric suction demonstrates gradual increase as the water content decreases. The fitted SWRCs using the Lu model show good agreement with measured suctions. The distinctions of both capillary and adsorptive water are also delineated in **figure 8**. The fitted adsorptive water and capillary water provide reasonable and quantitative assessment of the SWR behavior, and the maximum adsorptive water

FIG. 8 Comparison of measured matric suction for each soil sample at equilibrium of every step of drying with independently tested SWRCs by WP4C, and SWRCs fitting with model of Lu (2016): (*A*) Boulder clay (BoC), (*B*) Denver claystone (DCs), (*C*) Sanmenxia clay (SmC), and (*D*) Ningming clay (NmC).

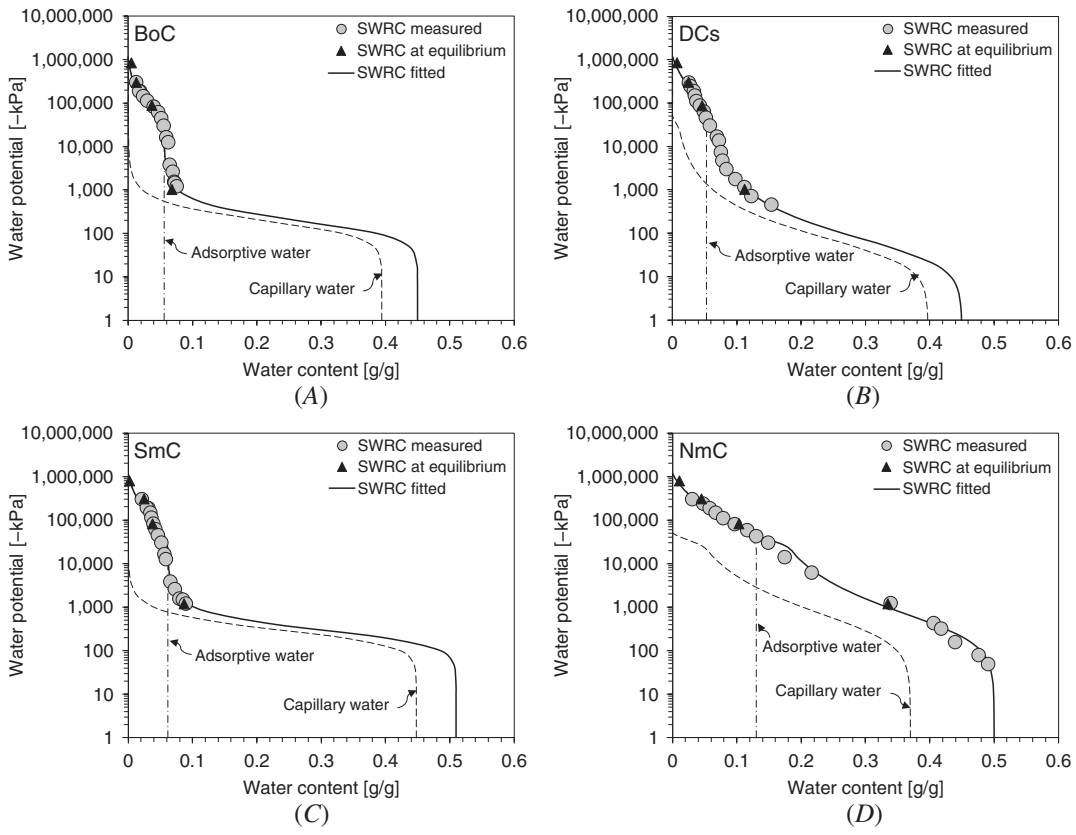

content can be numerically determined varying from 0.06 for low-expansive Sanmenxia clay to 0.13 for high-expansive Ningming clay.

Validation

The experimentally measured suction stress in low water content or high suction regime in this work was compared with previous results (Dong and Lu 2017) tested independently under room-dried conditions. In the previous testing procedure, no desiccant or dry air was used to dry the soil samples. The driest state was about 30 % (±10 %) RH and was in the range of 123–215 MPa of suction. Suction stress was determined using the radial stress obtained by particle image velocimetry technique (Lu and Kaya 2013). In the current experimental scheme, the extreme dry environment can be delivered by using activated MS to as low as 0.21 % of RH, and equivalently, total suction can be increased up to 850 MPa. In addition, the SSC-based suction stress calculation is simpler, compared with the previous method, without complicated image processing to compute the displacement vector field of each element of the sample surface.

The comparisons between SSCCs obtained by particle image velocimetry analysis in the previous study and SSCCs obtained by SSC analysis in the current study are presented in **figure 9**. The development of SSCCs with evolving volumetric water content are presented in **figure 9*A***. For Denver claystone, two independently tested samples have similar initial porosity around 0.53. The suction stress development shows an almost identical

FIG. 9 Comparisons of experimental results of suction stress measurements under high suction conditions with the results measured by previous drying cake method under room drying conditions for Denver claystone: (*A*) suction stress with varying water content and (*B*) suction stress with varying matric suction.

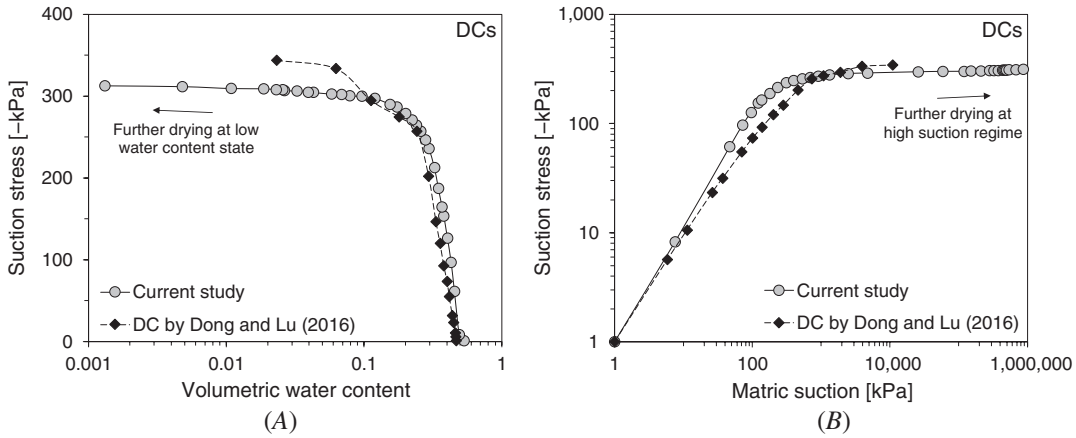

pattern as the water content decreases. Suction stress evolves 80 % of the minimum value to about −274 kPa as the water content decreases from 0.52 to 0.18. Below water content of 0.11, the suction stress stays more or less constant and continuously decreases as water content reduces to 0.001. Apparently, the previous technique can only dry Denver claystone to water content of 0.02; however, more data points have been collected in the current testing method from 0.02 of water content down to 0.001.

Another perspective with the relationships between suction stress and matric suction also demonstrates the advancement of the current technique compared with its predecessor, as shown in **figure 9*B***. Although the suction stress magnitude agrees well between the two measurement techniques, the deduced matric suction in the previous technique from suction stress using the effective degree of saturation is heavily restrained by its accuracy, and a very limited range of matric suction can be accessed. However, the concurrent measurements of suction stress and matric suction in this study using a well-controlled humidity environment overcome this limitation and provide much detailed information on SSCC and SWRC of soil in the high suction range. Particularly, the technique in the current study extends the upper bound of suction by hundreds of megapascals and makes 850 MPa experimentally achievable for unsaturated soil testing.

Conclusions

In this article, an environmental controlled chamber was modified and redesigned based on a previously established drying cake technique. MS were introduced into the testing system as powerful desiccants to achieve higher total suction up to 850 MPa. Four clayey soils representing low-expansive, expansive, and high-expansive soil were examined to establish the experimental procedures, including soil preparation, desiccant regeneration, drying process, volume and modulus measurement, and suction stress determination. Soil cake samples were prepared and desaturated stepwise, and equilibrium conditions were accomplished for each drying step. Saturated salt solutions were used conveniently for maintain the environment with RH from 99 to 6 %. Reactivated MS were deployed in the last drying step to achieve RH between 0.21 and 6 %, i.e., matric suction from 387 to 850 MPa.

Soil deformation was accurately monitored using a digital camera and image process technology. The elastic modulus was measured separately without disturbing the constraint-free drying cake sample. A simple bulk volume solution was used to determine suction stress from the SSC. The SWRCs were obtained by RH measurements in a high suction range and compared with independent matric suction measurements. The newly developed testing apparatus can successfully measure the SSC, SWRC, and suction stress characteristic curve. The experimental

results revealed new insights on hydrological and mechanical properties of expansive soils, particularly in the high suction range for adsorption water retention behavior. The new testing technology provided an effective tool to evaluate the mechanical properties of nearly fully dried soils and showed promising potential to develop a new testing standard for soil classification and soil property assessment.

ACKNOWLEDGMENTS

This research is sponsored by the National Science Foundation (CMMI-1363315, CMMI-1622781), National Natural Science Foundation of China (NSFC-51779254, 41572293), and Tsinghua University (SKLHSE-D-03). In addition, the Hundred Talents Program of the Chinese Academy of Sciences awarded to Y.D. is gratefully appreciated.

References

Abou Najm, M., R. H. Mohtar, J. Weiss, and E. Braudeau. 2009. "Assessing Internal Stress Evolution in Unsaturated Soils." *Water Resources Research* 45, no. 5 (May): W00C11. https://doi.org/10.1029/2007WR006484

Akin, I. D. and W. J. Likos. 2017. "Brazilian Tensile Strength Testing of Compacted Clay." *Geotechnical Testing Journal* 40, no. 4 (July): 608–617. https://doi.org/10.1520/GTJ20160180

Alonso, E. E., J.-M. Pereira, J. Vaunat, and S. Olivella. 2010. "A Microstructurally Based Effective Stress for Unsaturated Soils." *Géotechnique* 60, no. 12 (December): 913–925. https://doi.org/10.1680/geot.8.P.002

Alsherif, N. A. and J. S. McCartney. 2014. "Effective Stress in Unsaturated Silt at Low Degrees of Saturation." *Vadose Zone Journal* 13, no. 5 (May): vzj2013.06.0109.

Bishop, A. W. 1959. "The Principle of Effective Stress." *Teknisk Ukeblad* 106, no. 39: 859–863.

Dong, Y. and N. Lu. 2016. "Correlation between Small-Strain Shear Modulus and Suction Stress in Capillary Regime under Zero Total Stress Conditions." *Journal of Geotechnical and Geoenvironmental Engineering* 142, no. 11 (November): 04016056. https://doi.org/10.1061/(ASCE)GT.1943-5606.0001531

Dong, Y. and N. Lu. 2017. "Measurement of Suction Stress Characteristic Curve under Drying and Wetting Conditions." *Geotechnical Testing Journal* 40, no. 1 (January): 107–121. https://doi.org/10.1520/GTJ20160058

Greco, R. and R. Gargano. 2015. "A Novel Equation for Determining the Suction Stress of Unsaturated Soils from the Water Retention Curve Based on Wetted Surface Area in Pores." *Water Resources Research* 51, no. 8 (August): 6143–6155. https://doi.org/10.1002/2014WR016541

Khosravi, A., N. Alsherif, C. Lynch, and J. McCartney. 2012. "Multistage Triaxial Testing to Estimate Effective Stress Relationships for Unsaturated Compacted Soils." *Geotechnical Testing Journal* 35, no. 1 (January): 128–134. https://doi.org/10.1520/GTJ103624

Likos, W. J. and N. Lu. 2003. "An Automated Humidity System for Measuring Total Suction Characteristics of Clay." *Geotechnical Testing Journal* 28, no. 2 (June): 179–190. https://doi.org/10.1520/GTJ11321J

Likos, W. J., N. Lu, and W. Wenszel. 2011. "Performance of a Dynamic Dew Point Method for Moisture Isotherms of Clays." *Geotechnical Testing Journal* 34, no. 4 (July): 373–382. https://doi.org/10.1520/GTJ102901

Lu, N. 2016. "Generalized Soil Water Retention Equation for Adsorption and Capillarity." *Journal of Geotechnical and Geoenvironmental Engineering* 142, no. 10 (October): 04016051. https://doi.org/10.1061/(ASCE)GT.1943-5606.0001524

Lu, N. and Y. Dong. 2017. "Correlation between Soil-Shrinkage Curve and Water-Retention Characteristics." *Journal of Geotechnical and Geoenvironmental Engineering* 143, no. 9 (September): 04017054. https://doi.org/10.1061/(ASCE)GT.1943-5606.0001741

Lu, N. and Y. Dong. 2019. "Erratum for 'Correlation between Soil-Shrinkage Curve and Water-Retention Characteristics' by Ning Lu and Yi Dong." *Journal of Geotechnical and Geoenvironmental Engineering* 145, no. 8 (August): 08219002. https://doi.org/10.1061/(ASCE)GT.1943-5606.0002090

Lu, N., J. W. Godt, and D. T. Wu. 2010. "A Closed-Form Equation for Effective Stress in Variably Saturated Soil." *Water Resources Research* 46, no. 5 (May): W05515. https://doi.org/10.1029/2009WR008646

Lu, N. and M. Kaya. 2013. "A Drying Cake Method for Measuring Suction-Stress Characteristic Curve, Soil–Water-Retention Curve, and Hydraulic Conductivity Function." *Geotechnical Testing Journal* 36, no. 1 (January): 1–19. https://doi.org/10.1520/GTJ20120097

Lu, N., M. Kaya, and J. W. Godt. 2014. "Interrelations among the Soil-Water Retention, Hydraulic Conductivity, and Suction-Stress Characteristic Curves." *Journal of Geotechnical and Geoenvironmental Engineering* 140, no. 5 (May): 04014007. https://doi.org/10.1061/(ASCE)GT.1943-5606.0001085

Lu, N. and M. Khorshidi. 2015. "Mechanism for Soil-Water Retention and Hysteresis at High Suction Range." *Journal of Geotechnical and Geoenvironmental Engineering* 141, no. 8 (August): 04015032. https://doi.org/10.1061/(ASCE)GT.1943-5606.0001325

Lu, N. and W. J. Likos. 2004. *Unsaturated Soil Mechanics*. Hoboken, NJ: Wiley.

Lu, N. and W. J. Likos. 2006. "Suction Stress Characteristic Curve for Unsaturated Soils." *Journal of Geotechnical and Geoenvironmental Engineering* 132, no. 2 (February): 131–142. https://doi.org/10.1061/(ASCE)1090-0241(2006)132:2(131)

Lu, N., B. Wu, and C. P. Tan. 2007. "Tensile Strength Characteristics of Unsaturated Sands." *Journal of Geotechnical and Geoenvironmental Engineering* 133, no. 2 (February): 144–154. https://doi.org/10.1061/(ASCE)1090-0241(2007)133:2(144)

Lu, N. and C. Zhang. 2019. "Soil Sorptive Potential: Concept, Theory, and Verification." *Journal of Geotechnical and Geoenvironmental Engineering* 145, no. 4 (April): 04019006. https://doi.org/10.1061/(ASCE)GT.1943-5606.0002025

McKeen, R. G. 1992. "A Model for Predicting Expansive Soil Behavior." In *Seventh International Conference on Expansive Soils*, 1–6. Lubbock, TX: Texas Tech Univerity Press.

Oh, S., N. Lu, T.-Y. Kim, and Y. H. Lee. 2013. "Experimental Validation of Suction Stress Characteristic Curve from Nonfailure Triaxial K_0 Consolidation Tests." *Journal of Geotechnical and Geoenvironmental Engineering* 139, no. 9 (September): 1490–1503. https://doi.org/10.1061/(ASCE)GT.1943-5606.0000880

van Genuchten, M. T. 1980. "A Closed-Form Equation for Predicting the Hydraulic Conductivity of Unsaturated Soils." *Soil Science Society of America Journal* 44, no. 5 (September): 892–898. https://doi.org/10.2136/sssaj1980.03615995004400050002x

Zhang, C. and N. Lu. 2019. "Unitary Definition of Matric Suction." *Journal of Geotechnical and Geoenvironmental Engineering* 145, no. 2 (February): 02818004. https://doi.org/10.1061/(ASCE)GT.1943-5606.0002004